scientific reports

Check for updates

OPEN

Automatic detection of arrival time for noisy microseismic data using a transformed difference between multiwindow energy ratios method

Zhiyong Zhang[1]✉, Wen Cao[1], Shuailong Wang[1], Hewen Yan[1], Junwei Wang[2], Diego Arosio[3], Azadeh Hojat[4] & Luigi Zanzi[4]

Detection of arrival times of microseismic events is one of the most fundamental steps in the application of microseismic monitoring. However, accurately determining arrival time remains challenging due to low signal-to-noise ratio and the complexity of geological structures in microseismic monitoring. To address this, we propose a new arrival time detection strategy, which is implemented by using a transformed difference between multiwindow energy ratios method (TDER). First, we use a modified difference between multiwindow energy ratios (DER′) to characterize microseismic traces. Then, we introduce a detection method for detecting arrival times using a transformed DER′, i.e., TDER. The transforming process can extract the feature of arrival points in manual picking. To establish and validate the TDER method, we use pseudo-synthetic and field data. The method's sensitivity to varying noise levels was tested using pseudo-synthetic data combined with real noise. Two field datasets were collected from a microseismic monitoring system deployed on an unstable rock face and an active tomography survey on a mountain, respectively. This method demonstrated good performance in low signal-to-noise ratio (SNR) scenarios and outperformed traditional STA/LTA and the original DER picking methods with superior accuracy and fewer failed detection. We also examined how changes in parameters affect the TDER picking results. The developed method is an adaptive and nearly parameter-free method, which can be easily implemented.

Keywords Automatic picking, Microseismic monitoring, Multiwindow energy ratios, Detection method, Unstable rock face

Arrival picking of microseismic signals in engineering geology investigations is a fundamental step in data processing. Using arrival times, we can locate seismic events, analyze moment tensors and generate velocity models of investigated media[1–7]. Microseismic monitoring methods can be used as a useful tool to diagnose geological and engineering problems and are being increasingly applied in a wide range of fields[8], such as CO_2 storage in subsurface reservoirs[9,10], rock burst in underground engineering[11,12], hydraulic fracturing[13,14], slope engineering[15,16], hydropower stations[17,18], and geological hazards[19,20].

Traditionally, the arrival picking work was carried out manually by human operators to ensure the picking accuracy. However, manual picking is time-consuming and lacks the efficiency. Moreover, due to the different expertise, picking results obtained by different experts are inconsistent[21]. Therefore, development of automatic picking methods is quite necessary in reality. A number of approaches have been developed in recent decades to address varied practical demands, including Akaike information criteria (AIC) method[22,23], cross-correlation method[24,25], machine learning method[26](for example, PhaseNet[27], FilterPicker[28], PSpicker[29], CubeNet[30], EdgePhase[31], polarization analysis method[32], autoregressive method[33], higher-order statistics[34], (time-)frequency decomposition[35], and energy-based method[36,37]. However, these methods still face two main challenges in automatic picking. One is from the low signal to noise ratio (SNR) data. Noise can obscure arrivals

[1]School of Mining, Liaoning Technical University, Fuxin 123000, China. [2]School of Mapping and Geographical Science, Liaoning Technical University, Fuxin 123000, China. [3]Dipartimento di Scienze Chimiche e Geologiche, Universita degli Studi di Modena e Reggio Emilia, Modena 41125, Italy. [4]Dipartimento di Ingegneria Civile e Ambientale, Politecnico di Milano, Milan 20133, Italy. ✉email: zhiyongzhang@hotmail.com; zhiyong.zhang@polimi.it

and reduce algorithm accuracy. The other is from complex wavefields in microseismic monitoring process. Multipathing, diffraction, and varying amplitudes complicate arrival detection.

Among these methods, energy-based method is simple and computationally efficient, which leads it to be a widely used method. This method covers a group of variations, such as short- and long-term average ratio (STA/LTA)[38,39], modified energy ratio (MER)[40], improved MER (IMER)[41], the multi-nested windows method[42] and difference between multiwindow energy ratios (DER)[43]. Although DER method improves the accuracy by reducing the effect of noise, the picking strategy of thresholding is not accurate enough and always shows a delay compared with the manual picking time. Therefore, the pick error is still too large for microseismic data and the detection algorithms need to be improved.

In this paper, a new arrival time detection strategy, based on an energy analysis approach, was developed and implemented. The developed method exhibits high accuracy, even under low SNR conditions. Specifically, we initially use a modified DER (DER') to mitigate the deviations of picking induced by random noise and to accurately extract the transition from noise-dominated to signal-dominated segments. Then, we apply the new arrival time detection strategy by performing a transformation on DER' (TDER) to accurately identify arrival points. Both pseudo-synthetic and field data were applied to evaluate the approach. Sensitivity analysis was conducted on the TDER parameters, and the method was compared with the traditional STA/LTA and the original DER picking approaches.

Methodology

Multiwindow-based characteristic function

Multiwindow-based characteristic function is based on energy ratio method and uses more than two windows. In this study, we use a modified version of DER[43] (DER') with three windows to characterize microseismic data. The first window (W_1) is designed to be short to effectively capture the energy associated with the signal onset, whereas the second and third windows (W_2 and W_3, respectively) are configured with longer durations to better characterize the energy of pre-onset noise. Here we assume that t is any calculating point of a microseismic trace (Fig. 1a). W_1 starts at this point, while W_2 is placed before this point and is adjacent to the first window. W_3 is of equal length to W_2, but positioned ahead of the calculating point by a distance equal to the duration of W_1. We use the average energy in DER' instead of total energy applied in the original DER, in order to eliminate the effect of window length in the comparison of energies calculated by three windows. First, we define the average energies in W_1, W_2 and W_3 (E_1, E_2 and E_3, respectively) as follows:

$$E_1(t) = \sum_{i=t}^{t+L_{sw}-1} a^2(i) / L_{sw} \tag{1}$$

$$E_2(t) = \sum_{i=t-L_{lw}+1}^{t} a^2(i) / L_{lw} \tag{2}$$

$$E_3(t) = \sum_{i=t-L_{sw}-L_{lw}+1}^{t-L_{sw}} a^2(i) / L_{lw} \tag{3}$$

where $a(i)$ represents the amplitude of trace at a time i, L_{sw} represents the duration of W_1, and L_{lw} represents the duration of W_2 and W_3. The E_1, E_2 and E_3 were calculated from the starting point to the ending point of the trace (Fig. 1b). Then, two energy ratios between W_1 and W_2 ($ER_{1,2}$) and W_1 and W_3 ($ER_{1,3}$) are defined respectively as follows:

$$ER_{1,2}(t) = E_1(t) / E_2(t) \tag{4}$$

$$ER_{1,3}(t) = E_1(t) / E_3(t) \tag{5}$$

The $ER_{1,2}$ and $ER_{1,3}$ were calculated from the starting point to the ending point of the trace (Fig. 1c). Next, we simplify the original DER by setting the parameter α to 1. Then, DER' is calculated by using the difference between $ER_{1,3}$ and $ER_{1,2}$, as follows:

$$DER'(t) = ER_{1,3}(t) - ER_{1,2}(t) \tag{6}$$

The DER' was calculated from the starting point to the ending point of the trace (Fig. 1d).

The DER' shows similar variations across different trace positions compared with the original DER[43]. It is assumed that t_0 is the real arrival time and noise is random. If the calculating point is before the time t_0–L_{sw}, E_1, E_2 and E_3 indicate noise energy and they have similar values (Fig. 1b). In this situation, energy ratios $ER_{1,2}$ and $ER_{1,3}$ converge to 1 and the DER' tends to zero (Fig. 1c, d). When the calculating point lies within the interval from $t_0 - L_{sw}$ to t_0, the energy E_1 increases and attains higher values due to the presence of signal energy, whereas the values of E_2 and E_3 remain comparatively low because they are still representative of noise energy. Therefore, both $ER_{1,2}$ and $ER_{1,3}$ exhibit an increase and maintain comparable values. As a result, the DER' should not change too much and remains approximately zero if the noise is random. But for the case illustrated in Fig. 1d, the DER' exhibits a marginal increase above zero (with values of about 20) at 1800 ms due to the fluctuation of noise (Fig. 1a). If the calculating point advances beyond t_0, E_1 has a relatively large value because the associated window fully covers the signal. W_2 partially captures signal energy and E_2 increases, whereas W_3 continues to exclusively capture noise energy and E_3 value remains small. Thus, $ER_{1,3}$ becomes significantly greater than $ER_{1,2}$, resulting in a rapid increase in DER' values. The DER' not only effectively reduces the impact of noise, but also obviously enhances the presence of the arrival time. Because of the distinct and observable feature of a

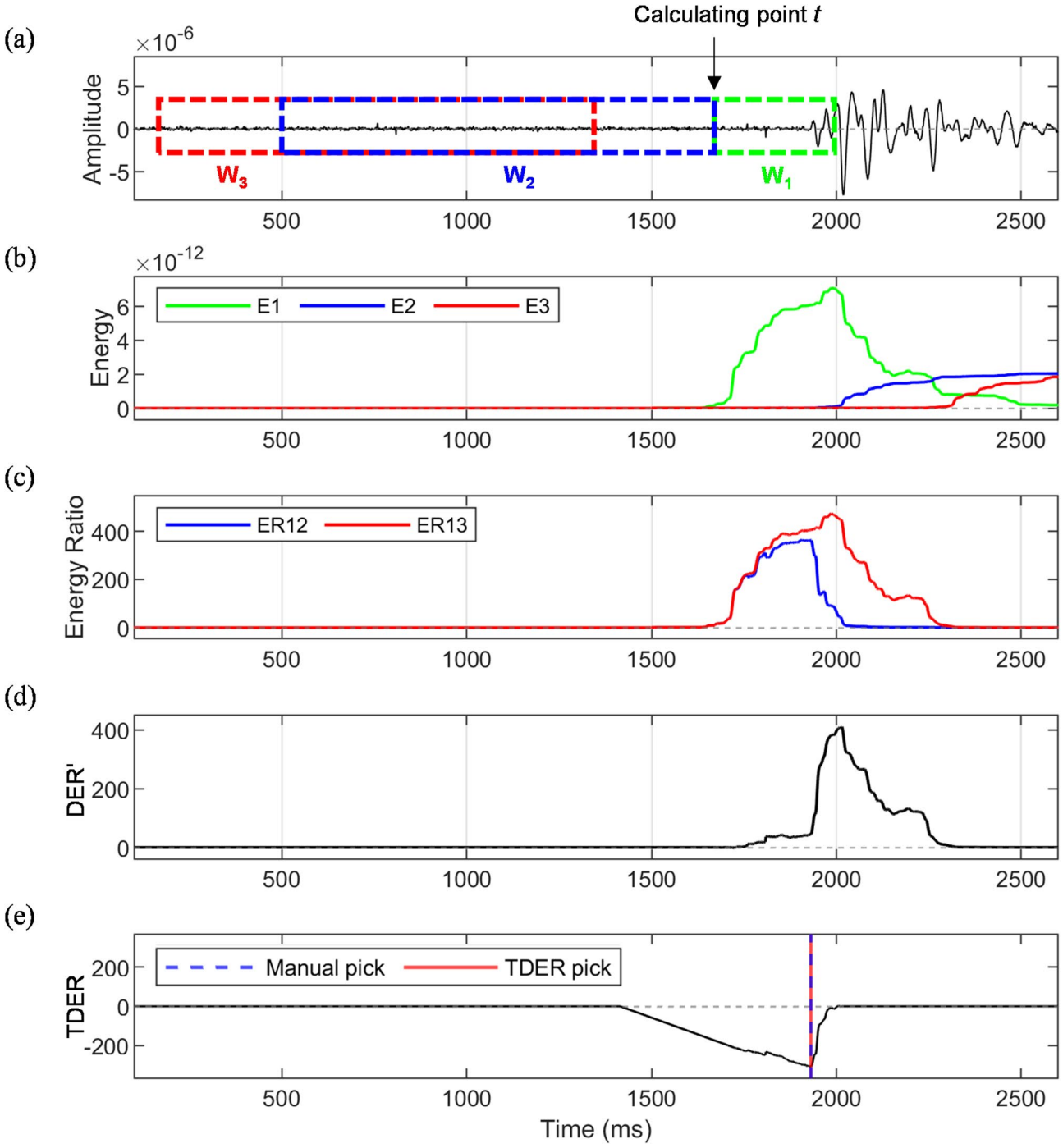

Fig. 1. Process of generating DER' and TDER. (**a**) A microseismic trace and the three windows used to calculate DER' (L_{sw} = 0.3 s, L_{lw} = 1.2 s). (**b**) Energies in three windows (E_1, E_2 and E_3 are energies in W_1, W_2 and W_3, respectively). (**c**) Energy ratios ($ER_{1,2}$, energy ratio between W_1 and W_2; $ER_{1,3}$, energy ratio between W_1 and W_3). (**d**) DER', difference of energy ratio between $ER_{1,3}$ and $ER_{1,2}$. (**e**) TDER, transformed characteristic function for detecting arrival time. The red vertical line indicates the automatic pick at minimum of TDER and blue vertical dashed line indicates the manual pick.

rapid increase in the DER' at the arrival time, the proposed function is able to enhance picking accuracy. Next, we describe the detection approach of the arrival time at the beginning of the rapid increase of DER'.

Detection of arrival time

Besides the generation of characteristic function for the seismic trace in energy-based picking methods, another critical aspect is how to determine the arrival times of signals[44]. Different from the thresholding used by the original DER to detect the arrival time, we propose a new detection strategy by performing a transformation

to the abovementioned DER'. If the automatic pick coincides with the start of the sharp rise in DER', prior to reaching its highest point, the optimal matching with manual picks can be achieved, based on the experience derived from manual picking practices. Considering that there are no straightforward mathematical techniques available to directly identify this shift, the transformation of DER' (TDER) aims to achieve this function and effectively pinpoint the arrival time.

The transformation removes a linear trend from DER' in the window of length $2L_{sw}$ before the maximum point of DER', as a result, the window's initial and final values turn to be zero. Meanwhile let other values out of the window be zero (Fig. 1e). In this way, the arrival time becomes global minimum of the TDER'. TDER' is defined as follows:

$$\mathrm{TDER}\,(t) = \begin{cases} DER\prime\ (t) - [a\,(t - (t_m - 2\mathrm{L_{sw}})) + b]\,, & t \in [t_m - 2\mathrm{L_{sw}},\ t_m] \\ 0, & others \end{cases}$$

$$with \begin{cases} a = \frac{\mathrm{DER}\prime\,(t_m) - \mathrm{DER}\prime\,(t_m - 2\mathrm{L_{sw}})}{2L_{sw}} \\ b = DER\prime\ (t_m - 2\mathrm{L_{sw}}) \end{cases} \tag{7}$$

where t_m is the time when DER' is highest. Picking the minimum of TDER gives a good estimate of arrivals (Fig. 1e).

We illustrate the processing implementation of using the window from t_m-$2L_{sw}$ to t_m for the transformation. A synthetic example showing the significance and implications of the transformation is presented in Fig. 2. A stationary noise segment and a stationary signal segment are depicted in Fig. 2a-b, respectively and the superposition of the signal in Fig. 2a and the noise Fig. 2b is shown in Fig. 2c. Figure 2d-e show the DER' graph and TDER when L_{sw} and L_{lw} are set to 0.3 s and 1.2 s, respectively. Ideally, if a seismic recording is segmented into stationary signal and noise, based on the analysis of the previsou section 'Multiwindow-based characteristic function', DER' reaches its maximum at time t_0+L_{sw} (Fig. 2d). By using the transformation window of $2L_{sw}$, t_0 is at the middle point of the window between t_m-$2L_{sw}$ and t_m. And the DER' value at t_0 is transformed to be the minimum, i.e. the minimum TDER (Fig. 2e). The minimum TDER is the middle point of $2L_{sw}$ corresponding to the very starting point of DER'. Figure 2f-g show the DER' graph and TDER when L_{sw} and L_{lw} are set to 0.5 s and 0.8 s, respectively. As the windows of L_{sw} and L_{lw} vary, the automatic pick using TDER in Fig. 2g maintains optimal accuracy. In reality, seismic recordings are not stationary signal and noise and the recognized picking points are not at the middle points of the transformed window, but these points are still located in the window from t_m-$2L_{sw}$ to t_m.

Results and discussion

Verification and experiments using pseudo-synthetic data

In this section, we investigated the accuracy of TDER by using pseudo-synthetic data with different noise levels. The pseudo-synthetic data were generated by adding different levels of noise to a field waveform. First, we selected a microseismic trace exhibiting a high SNR. Before adding noise and arrival time picking, a zero-phase 10 Hz high-pass filter was applied on this trace to remove low frequency fluctuations. The SNR of each signal was calculated as follows:

$$SNR\,(t_0) = 10 \times \log_{10} \frac{E_1\,(t_0)}{E_2\,(t_0)} \tag{8}$$

where t_0 was the manual pick of arrival time; E_1 and E_2 were the average energies in W_1 and W_2, respectively, defined by Eqs. (1) and (2). The selected high-SNR microseismic trace is shown in Fig. 3a. Then we extracted a section of real noise from field data that were used in the following section 'Microseismic data'. In order to simulate different levels of noise, the real noise was artificially adjusted to be with different standard deviations (STDs) corresponding to 5%, 10%, and 20% of the maximum amplitudes of the selected microseismic trace. Next three levels of noise were subsequently added to the microseismic trace (Fig. 3e, i, m).

In order to show the improvement of picking accuracy, TDER method was compared with the traditional STA/LTA and the original DER methods. For STA/LTA method[38], L_{sw} and L_{lw} were used to calculate the STA and LTA, respectively. The threshold of STA/LTA was snr, which is a constant parameter set by the user as the signal-to-noise ratio corresponding to the minimum-energy signal that can be identified by using the specified threshold. The DER is defined by Eqs. (9)–(14), and the threshold of the arrival time is defined by Eq. (15)[43]:

$$E_1\,(i) = \sum\nolimits_{j=i}^{i+L_{sw}} a_j^2 \tag{9}$$

$$E_2\,(i) = \sum\nolimits_{j=i-L_{lw}}^{i} a_j^2 \tag{10}$$

$$E_3\,(i) = \sum\nolimits_{j=i-L_{sw}-L_{lw}}^{i-L_{sw}} a_j^2 \tag{11}$$

$$ER_{12}\,(i) = E_1\,(i)\,/E_2\,(i) \tag{12}$$

$$ER_{13}\,(i) = E_1\,(i)\,/E_3\,(i) \tag{13}$$

$$DER\,(i) = \frac{ER_{13}\,(i)}{\alpha} - ER_{12}\,(i) \tag{14}$$

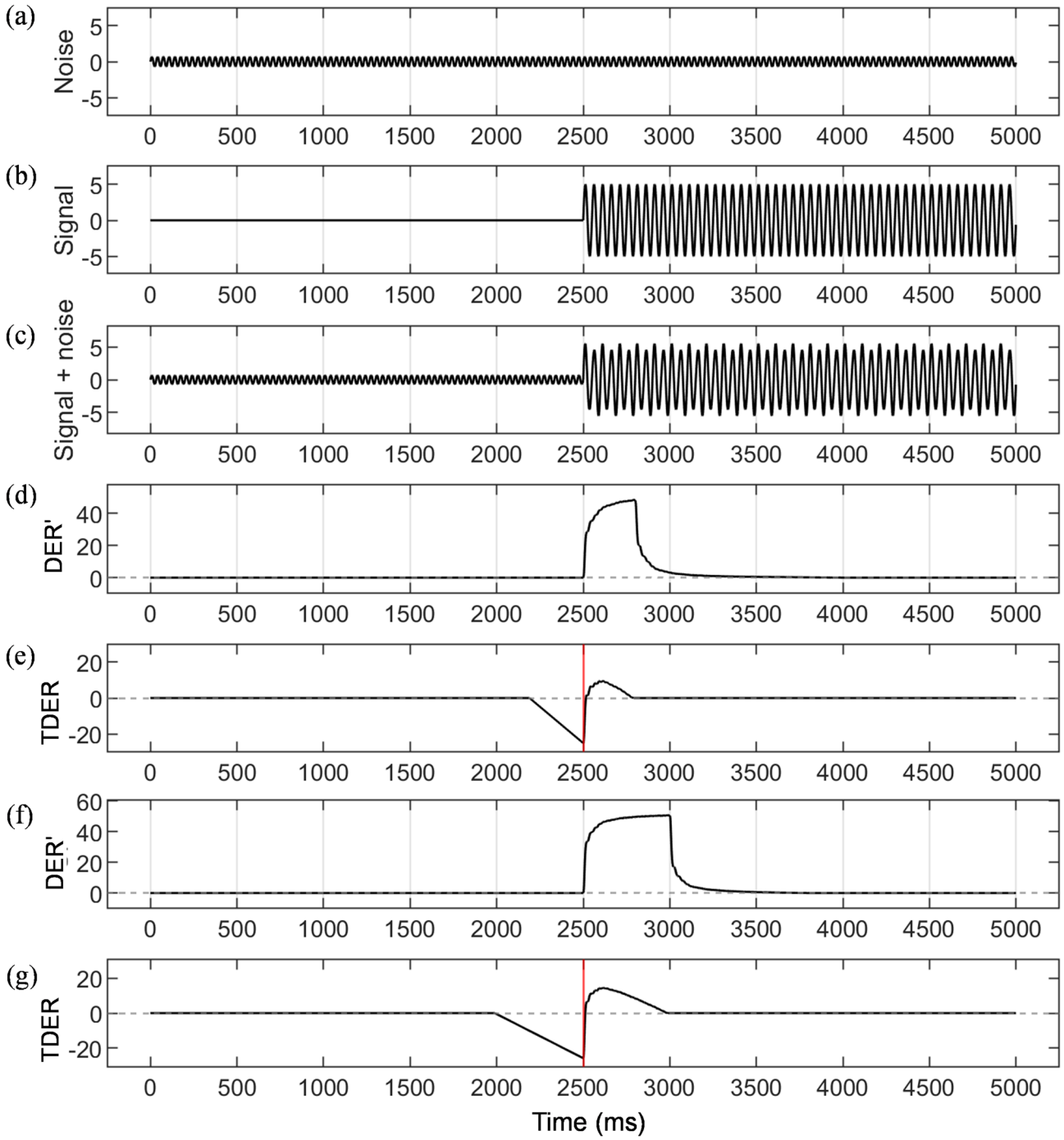

Fig. 2. Process of generating stationary signals and noise and the performance of TDER picking. (**a**) Synthetic stationary noise. (**b**) Synthetic stationary signal. (**c**) Superposition of (**a**) and (**b**). (**d**)-(**e**) Computed DER' and TDER when L_{sw}=0.3 s and L_{lw}=1.2 s. (**f**)-(**g**) Computed DER' and TDER when L_{sw}=0.5 s and L_{lw}=0.8 s. The sample frequency is 1000 Hz. Red vertical lines in (**e**) and (**g**) show the automatic picking points at minimum of TDER.

$$Threshold:\ DER(i) \geq\ snr \bullet\ R\left[\frac{1}{\alpha} - \frac{1}{(snr-1)\,R+1}\right] \tag{15}$$

where α is a parameter that stabilizes the DER and is slightly larger than 1; R is the ratio of L_{sw} to L_{lw} ($R = L_{sw}/L_{lw}$). In comparison, the parameters L_{sw}, L_{lw}, snr and α were assigned values to 0.3 s, 1.2 s, 1.5 and 1.05, respectively, for the above-mentioned methods.

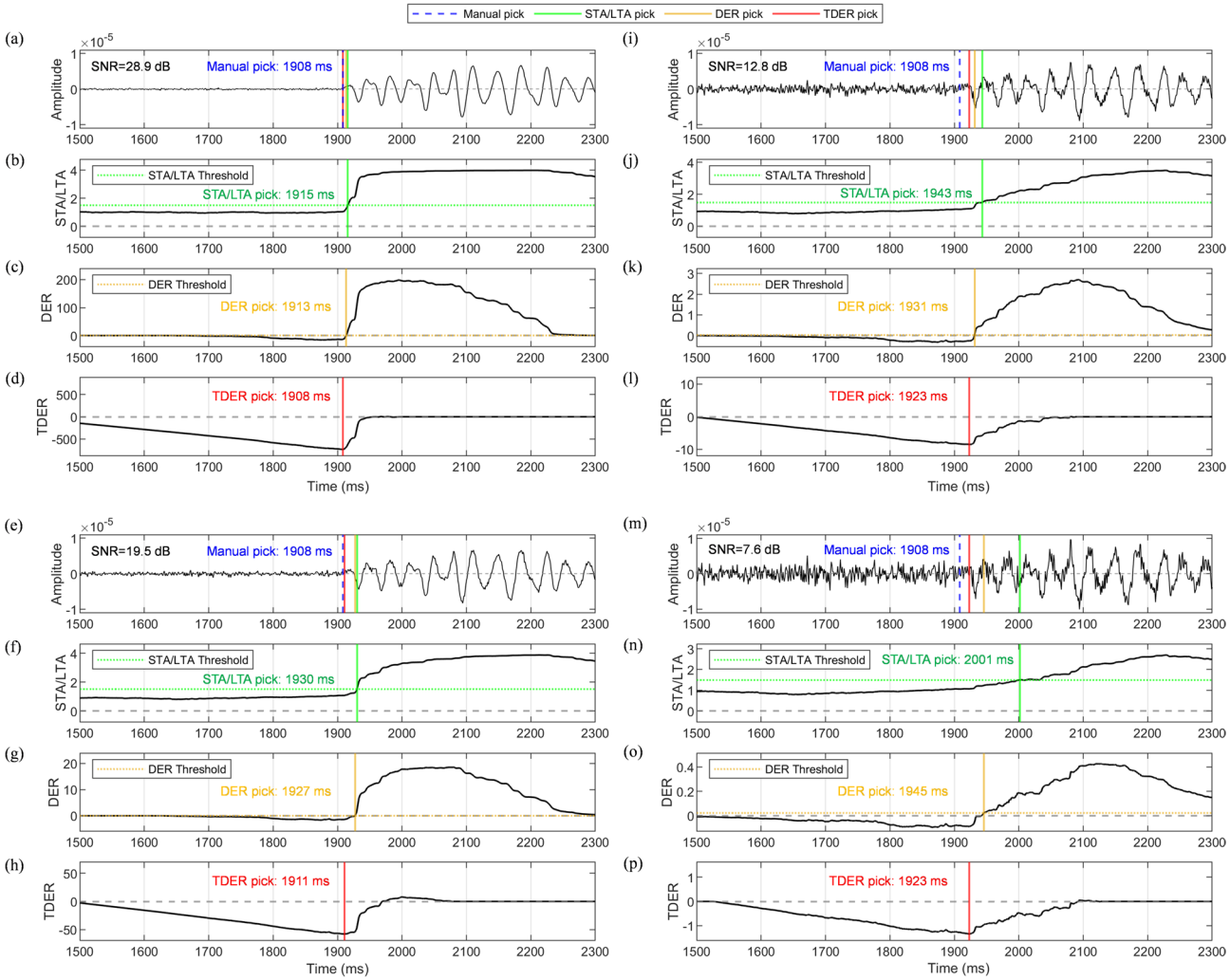

Fig. 3. Picking performance of three methods at different noise levels. (**a**)-(**d**) A microseismic trace followed by the associated STA/LTA, DER and TDER. (**e**)-(**h**), (**i**)-(**l**) and (**m**)-(**p**) Seismic recordings incorporating adjusted noise with STDs corresponding to 5%, 10%, and 20% of the maximum amplitudes of the original trace, respectively, followed by the associated STA/LTA, DER and TDER. The manual, STA/LTA, DER, and TDER picks are represented by the vertical lines that are blue dashed, green solid, yellow solid and red solid, respectively (L_{sw} = 0.3 s, L_{lw} = 1.2 s).

The original trace, its STA/LTA, DER and TDER are presented in Fig. 3a-d. In this case, the arrival time of the seismic recording is clear, both STA/LTA and DER values increase after passing through the arrival time. However, the thresholds of the two methods cannot capture the beginning of the increase and work only when the STA/LTA and DER increase enough to meet the thresholds. Therefore, STA/LTA and DER detect the arrival time a few milliseconds later than the manual pick due to the drawback of the threshold strategy. Conversely, TDER overcomes the drawback of the threshold strategies and has a good adaptability by transforming the beginning of the increase at the arrival time to the minimum and then detecting it easily. Thus, the TDER picks a marked minimum that coinsides with the manual pick.

Figure 3e-h show the data including the adjusted noise with a STD of 5% of the highest amplitude of the original data, followed by its STA/LTA, DER and TDER. Due to the presence of noise, the increase of STA/LTA is much slower and so is that of DER. Based on the threshold strategy, both STA/LTA and DER picks perform worse with a larger delay of around 20 ms. For TDER, the picking time is just slightly delayed compared to the manual pick with the picking error of 3 ms. The datasets containing the adjusted noise with STDs corresponding to 10% and 20% of the greatest amplitudes of the original data, respectively, are as shown in Fig. 3i-l and Fig. 3m-p. With the rise of noise level, the arrival time of the signal becomes more obscured and the detection of arrival time is more difficult. The picking errors of STA/LTA and DER increase more quickly than that of TDER. Nevertheless, the TDER shows the best performance with the minimum error among three methods.

In order to assess the results' statistical robustness, we applied a total number of seven noise levels and three high-SNR microseismic traces. The three selected microseismic traces, including the one used in the previous test, had the SNR of 28.9 dB, 25.6 dB and 21.5 dB, respectively. We extracted the real noise from microseismic

data that were used in the following section 'Microseismic data' and the number of real noise is 500. Seven noise-level tests (Test1-Test7) were performed by using the real noise and six adjusted real noise with STDs corresponding to 5%, 10%, 20%, 30%, 40% and 50% of the maximum amplitudes of each microseismic trace. For each microseismic trace, the test at each noise level was repeated 500 times by using the 500 noise. The picking accuracy was evaluated by computing the mean absolute difference (MAD) between each method's pick and manual pick, the STD of the difference and the average SNR of the microseismic trace with noise.

The comparison of picking results with different noise levels was shown in Fig. 4. As the noise level increases, the average SNR of data decreases correspondingly for three traces, and the picking performance of all three methods deteriorates. In the case of Trace1 (Fig. 4a), both MAD and STD of STA/LTA and TDER picks show the increasing trend as the noise level increases. However, for DER picks, MAD and STD fluctuate first and then increase with the noise levels from low to high. Moreover, MAD of DER picks is larger than MAD of STA/LTA when SNR is over 18 dB. The reason would be that DER method is highly sensitive to the irregular noise and small fluctuations could be recognized as the arrival time when SNR is relatively large (Fig. 4b-e). When the SNR is lower than 5 dB, the picking error increases rapidly for all three methods, especially for STA/LTA and DER methods.

For Trace2 and Trace3 (Fig. 4f-g), the variations of MAD and STD show similar results compared with those for Trace1. Since the original Trace2 and Trace3 have relatively lower SNR compared with the original Trace1, the performance of DER method gets worse when SNR is relatively large. By comparison, we can see that TDER method always gives the lowest MAD and STD at different noise levels.

It should be mentioned that noise levels were tested up to 50% of the greatest amplitude of the original data for Trace1 and Trace2, but only up to 30% for Trace3. Beyond this level, the signal was effectively concealed (SNR

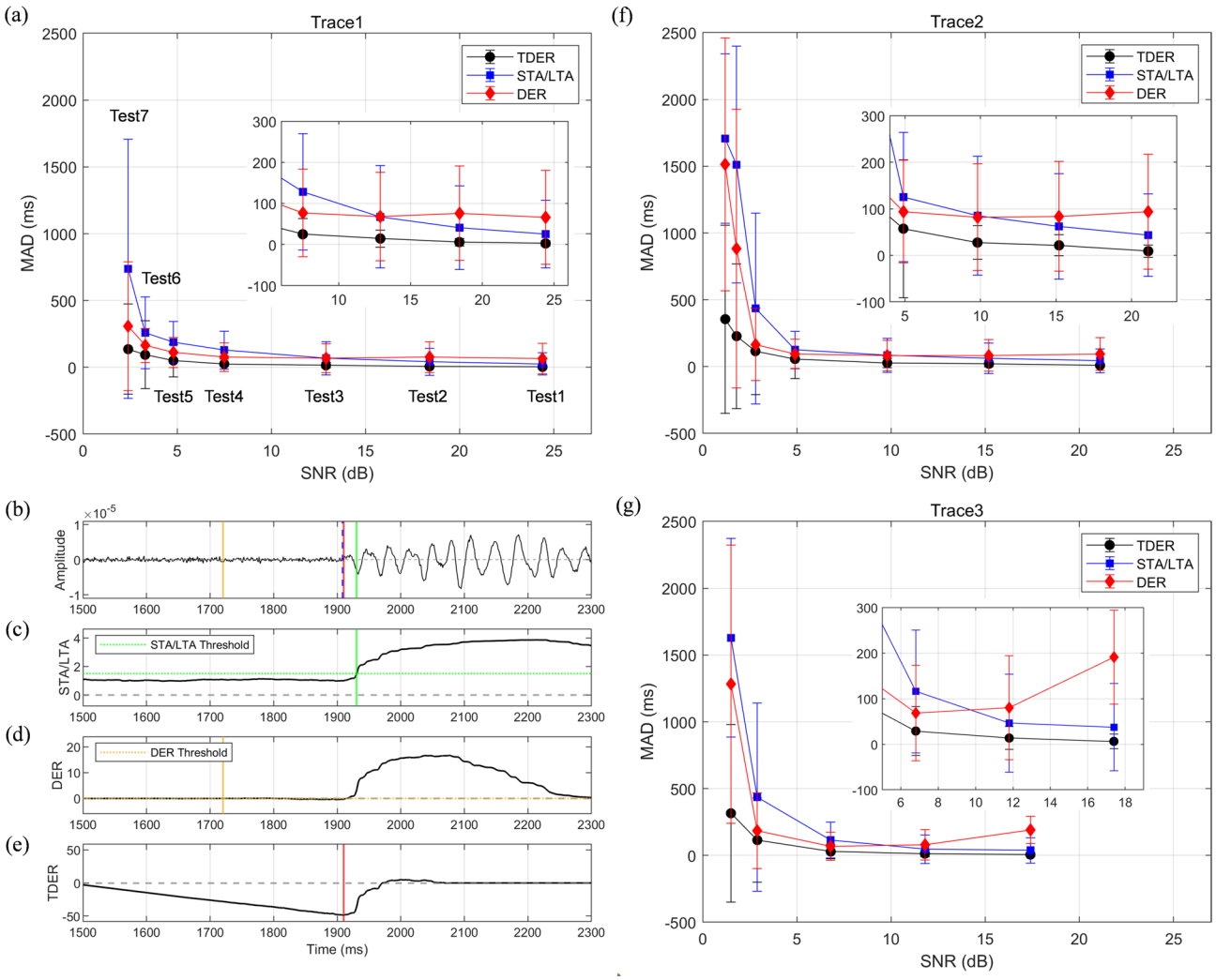

Fig. 4. Comparison of picking results with different noise levels. MAD and STD of three methods by using (**a**) Trace1. Zoomed windows are displayed to show the detailed differences. (**b**)-(**e**) Example of Seismic recording (Trace1) incorporating adjusted noise with STD corresponding to 5% of the maximum amplitudes of the original trace, respectively, followed by the associated STA/LTA, DER and TDER. MAD and STD of three methods by using (**f**) Trace2 and (**g**) Trace3. Zoomed windows are displayed to show the detailed differences.

is around 1 dB), resulting in unacceptably low picking accuracy where manual identification of arrival times became impossible.

The influence of noise on picking accuracy can also be evaluated by the ratio of delayed picks compared with manual picks. Here we use the results of TDER method in previous tests due to its best picking performance among three methods (Fig. 5). Overall, the ratio of delayed picks first increases and then decreases when the SNR decreases. The results could be caused by the noise level with respect to the onset signal.

For Trace1, in Test1 using real noise, the noise that is added to the signal is quite small and its influence on the first crest of the onset can be ignored. Thus, TDER picks can be almost equally located before or after the manual pick, and the ratio of delayed picks is around 50%. When the noise level is 5% of the original data's highest amplitude in Test 2, the noise that is added to the signal is relatively small and could not totally obscure the first crest of the onset as seen in Fig. 3e. Therefore, most of TDER picks are just a little after the manual pick but still before the first crest of the onset. In Test3, the noise level increases and the added noise could nearly obscure the first crest of the onset as seen in Fig. 3i. Thus, TDER picks are mostly after the first crest of the onset and most of them are stopped at the beginning of the first trough of the onset because of the large amplitude of the first trough compared to this noise level. Similar analysis can be done for Test4 to Test7 by comparing the noise and the onset signal. With increasing noise level, the tests result in relatively lower ratios of delayed picks. Because the high noise level is, the more of the onset signal can be obscured by noise so that the noised signal is less likely to be recognized successfully and more possible to be recognized as noise. Trace2 and Trace3 show similar results and the differences could be caused by different onset signals of three traces.

The picking accuracy is an important parameter for seismic event localization to evaluate and explain the location accuracy in future data processing and analysis[2,45,46]. By using the tests of noise sensitivity, we can give an estimation of picking accuracy using TDER for traces with different noise levels. One available way would be using the SNR for estimating the picking uncertainty. First, based on the pseudo-synthetic tests, we can obtain the relationship between SNR and STD of picking error by fitting the picking data. Then we calculate the SNR

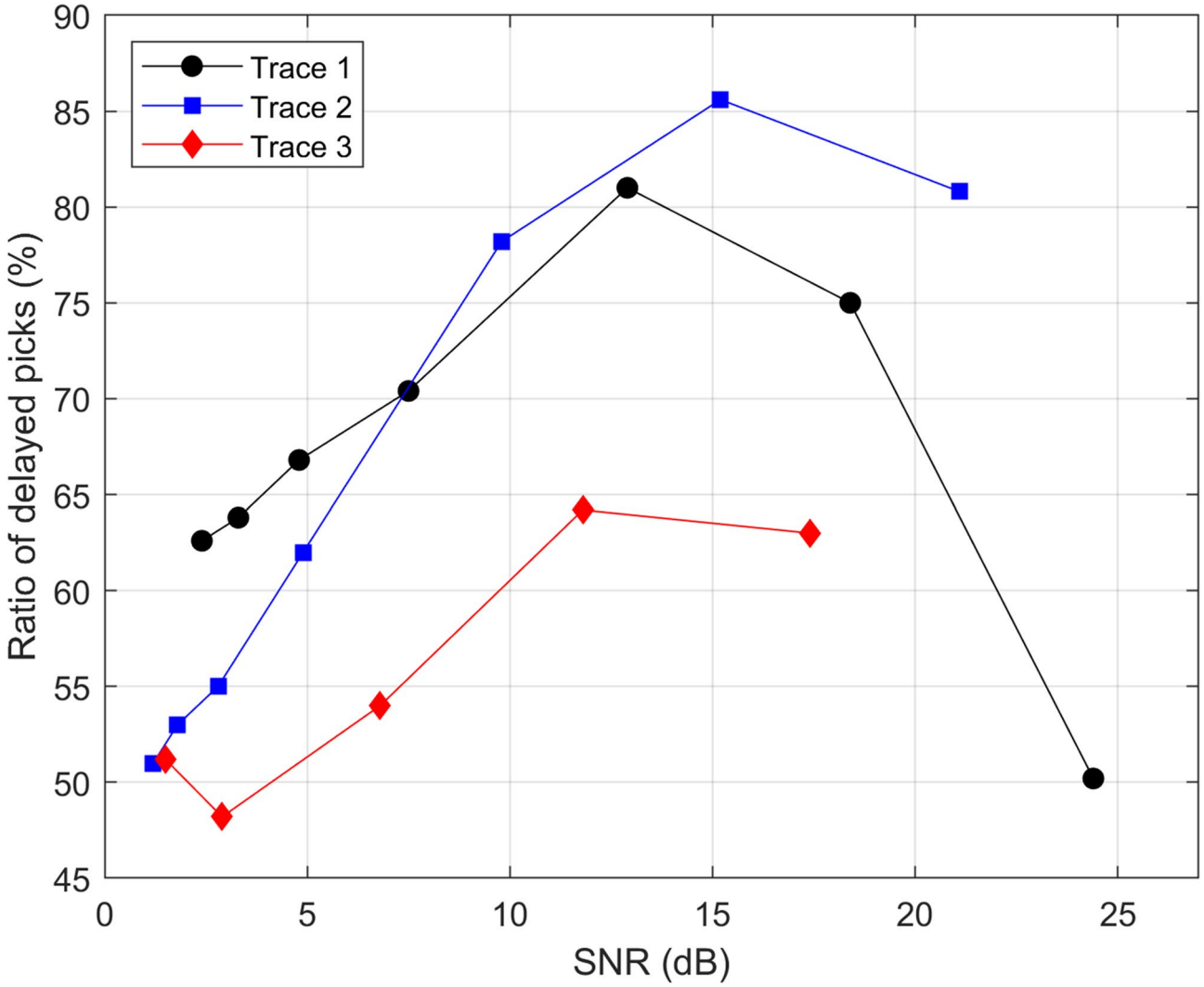

Fig. 5. Ratio of delayed picks of TDER method with different SNRs for three traces.

for field data, and each SNR corresponds to an STD of picking error. Thus, the STD of picking error can be used as an estimate of the picking uncertainty. To justify this method, a broader quantitative evaluation in future research would be necessary.

Verification and experiments using field data

Overview of field data

Microseismic data Mount San Martino is located in northern Italy with an unstable limestone rock face, measuring around 330 m in height, on its southern side. A microseismic system including five 3-component (3 C) geophones has been monitoring the rock face since 2013 (Fig. 6a-b). Using a predetermined triggering technique, each geophone has the ability to capture microseismic events at a sampling frequency of 1 kHz. Additional details regarding the data acquisition process are available in the referenced literature[5–7,47]. In this paper, we used the data monitored during 2013 to 2016 with 155 microseismic events, which were related to rockfalls or fracture propagation[47]. Before arrival time picking, a zero-phase 10 Hz high-pass filter was performed on the dataset to remove low frequency fluctuations. Then the arrival times of the events were manually picked. Given that each geophone records 3 C seismic traces, all components were separately picked. In the end, 1275 traces from 85 events were able to be manually picked and these traces were utilized in the proposed automatic picking method. The range of SNR of the 1275 microseismic traces is 1.0 to 48.4 dB with the mean of 13.2 dB. The dominant frequencies of the used microseismic data have a mean of 40.6 Hz and an STD of 11.2 Hz. The distribution of microseismic data is shown in Fig. 6c. The microseismic data were used for the following sections 'Comparative analysis with STA/LTA and DER methods' and 'Sensitivity analysis and parameter selection'.

Active tomography data The active tomography survey was performed on the top of a mountain (Fig. 7a). A 24-channel Geode recording system was used for data acquisition. Twenty-four vertical geophones were deployed and 26 shots were performed on nine source positions. The sampling frequency is 4000 Hz. The data were picked manually and, and we were able to manually pick 503 arrival times from 624 seismograms. The range of SNR of the 503 tomographic traces is 5.4 to 57.5 dB with the mean of 29.5 dB. The dominant frequencies of tomographic data have a mean of 71.2 Hz and an STD of 13.2 Hz. The distribution of tomographic data is shown in Fig. 7b. The active tomography data were used in the following section 'Sensitivity analysis and parameter selection'.

Comparative analysis with STA/LTA and DER methods

The TDER method not only benefits from DER to mitigate the influence of noise, but also enhances picking accuracy through the implementation of the novel detection strategy compared to other energy-based picking techniques. The improvement in picking accuracy was also demonstrated for the microseismic data by comparing the TDER picking results with those of the traditional STA/LTA and the original DER methods. In comparison, the parameters L_{sw}, L_{lw}, snr and α were assigned values to 0.3 s, 1.2 s, 1.5 and 1.05, respectively, for the above-mentioned methods (Fig. 8).

Figure 8a shows a signal with high SNR and its picking results. The arrival time of the seismic recording is clear, both STA/LTA and DER values increase after passing through the arrival time. However, the thresholds of the two methods cannot capture the beginning of the increase and work only when the STA/LTA and DER

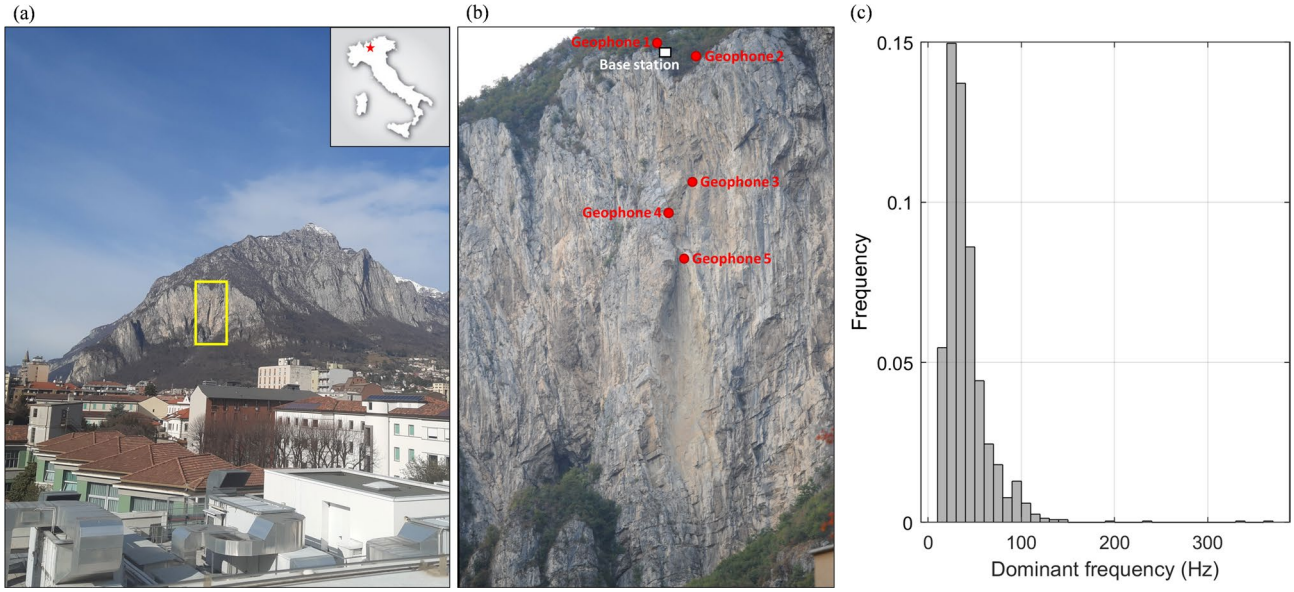

Fig. 6. (**a**) Mount San Martino's unstable rock face, viewed from the south. (**b**) Microseismic system deployed on the rock face. White square indicates the base station's position and red circles show the positions of five 3 C geophones. (**c**) Distribution of dominant frequency of microseismic data.

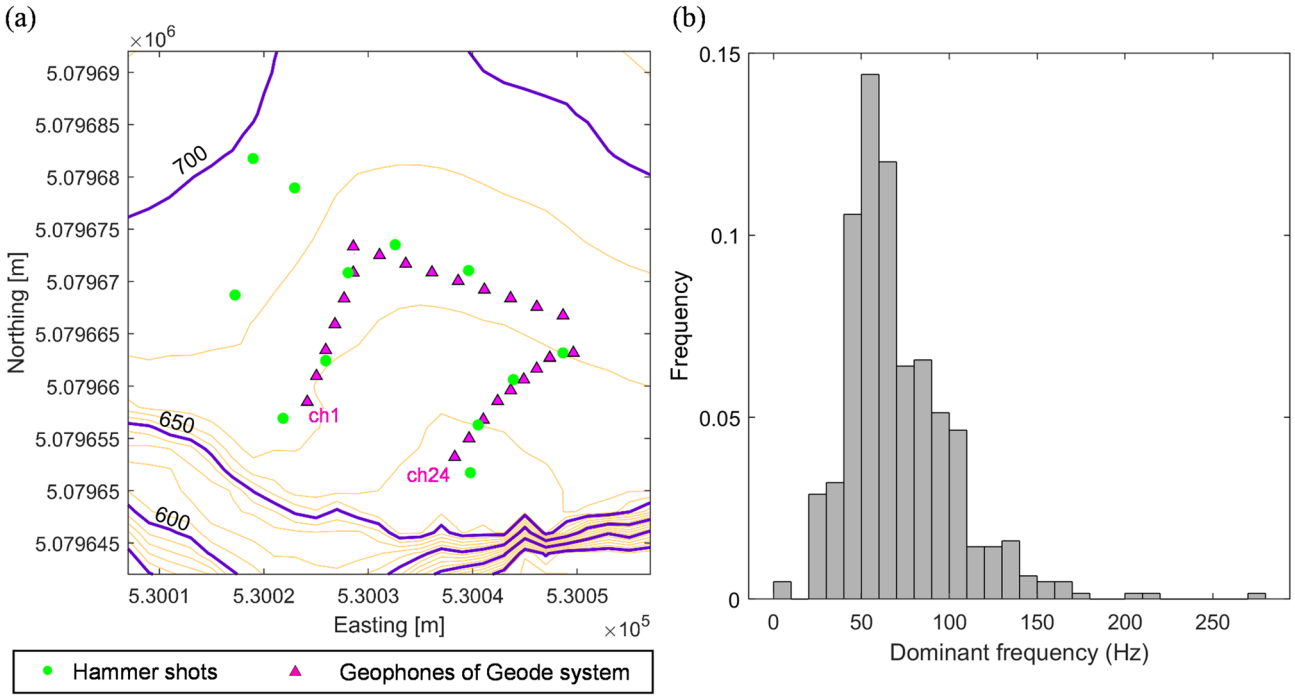

Fig. 7. (**a**) Layout of the tomographic survey on a mountain. Contours are in meters above the sea level. (**b**) Distribution of dominant frequency of active tomographic data.

increase larger enough to meet the thresholds. Therefore, STA/LTA and DER detect the arrival time later than the manual pick due to the drawback of the threshold strategy (Fig. 8b-c). This issue frequently occurs when the arrival times are picked. Conversely, TDER overcomes the drawback of the threshold strategies and has a good adaptability by transforming the beginning of the increase at the arrival time to the minimum and then detecting it easily. Thus, the TDER picking result remain at a similar level to that of the manual picking (Fig. 8d).

This TDER also works well for noisy data. Figure 8e shows a signal with relatively low SNR and its picking results. Figure 8f-g show that the increase of STA/LTA is much slower and so is that of DER. Based on the threshold strategy, both STA/LTA and DER picks are later than the manual picks. In contrast, the TDER captures the transition point from noise to the signal and its picking is very similar to the manual one (Fig. 8h).

Figure 8i shows a signal with fluctuations in noise and its picking results. STA/LTA cannot pick the arrival time correctly due to significant fluctuations in the presence of noise (Fig. 8j). A similar result is observed with DER method (Fig. 8k). TDER got the picking result similar to the manual one and showed the flexibility and adaptivity for the signal with fluctuation noise (Fig. 8l). Therefore, regardless of the noise level, TDER performs better than STA/LTA and DER.

We use more data to show the statistical comparison between the results of the three methods. In total, 1275 microseismic traces that were picked manually were used for the comparison. The results are shown in Table 1, that lists MAD and STD between each method and manual picking results. For STA/LTA and DER methods, since the greatest value of the STA/LTA and DER did not surpass the threshold, several picks were not identified. In contrast, TDER method detected all the picks. Also, TDER method gives the lowest MAD and STD compared to the other two methods.

Sensitivity analysis and parameter selection

Parameter setting is crucial in the arrival picking procedure[48,49]. In this section, we test the effects of L_{sw}, L_{lw}, as well as the length of transformation window. In the TDER method, the first window with the length of L_{sw} is used to estimate the energy of the signal in microseismic recordings. Reducing the window length enhances sensitivity to transient signals and noise spikes, improving the accuracy of arrival time picking while simultaneously increasing the probability of false detections. As such, selecting the value of L_{sw} entails a trade-off between increasing picking accuracy and reducing false alarms. The intended signal's frequency determines the optimal value of L_{sw}. In practice, L_{sw} needs to span a minimum of one period and be sufficient to encompass the onset energy.

We proposed a method to determine the short window length (L_{sw}) by analyzing how the onset energy changes with L_{sw}. For each trace, we calculate the energy in the L_{sw}-length window just before the peak amplitude. As L_{sw} increases, the window initially captures mostly signal energy, but after a certain point, it starts including noise. This is reflected by a sharp drop in energy followed by a gradual decline. We interpret the inflection point in this energy curve as the appropriate L_{sw} that captures only the onset. For our microseismic data, variations of the average onset energy with different L_{sw} are calculated and shown in Fig. 9a. When L_{sw} is 0.1 to 0.3 s, onset energy decreases rapidly and linearly, which shows that the onset energy mainly locates in these window lengths

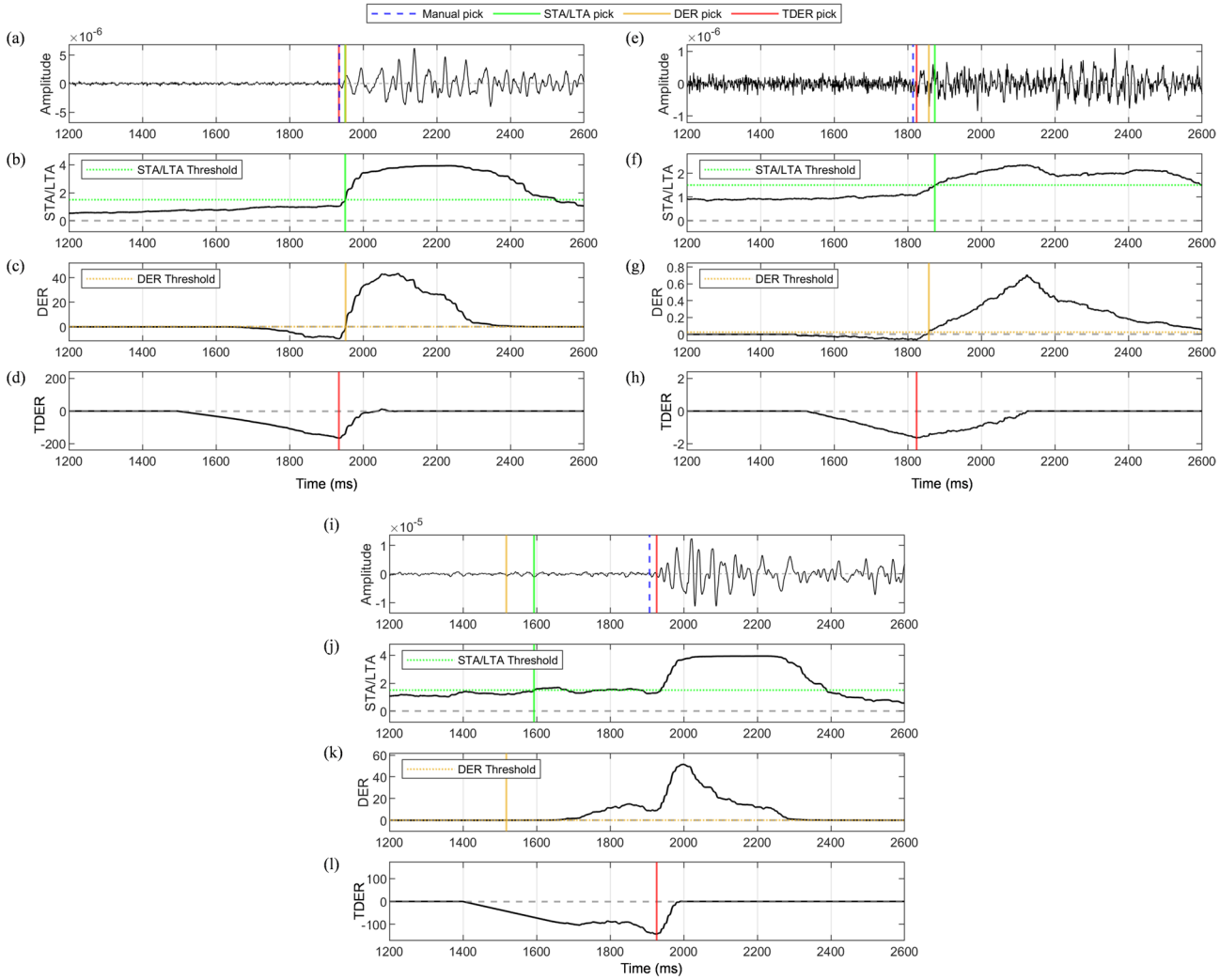

Fig. 8. Examples of picking results for comparison. (**a**), (**e**) and (**i**) Three raw microseismic recordings with manual, STA/LTA, DER and TDER picks. (**b**), (**f**) and (**j**) STA/LTA threshold and picks of (**a**), (**e**) and (**i**), respectively. (**c**), (**g**) and (**k**) DER picks of (**a**), (**e**) and (**i**), respectively. (**d**), (**h**) and (**l**) TDER picks of (**a**), (**e**) and (**j**), respectively. The manual, STA/LTA, DER, and TDER picks are represented by the vertical lines that are blue dashed, green solid, yellow solid and red solid, respectively (L_{sw} = 0.3 s, L_{lw} = 1.2 s).

Method	Number of success detections	Number of failed detections	MAD (ms)	STD (ms)
STA/LTA	1268	7	155.0	148.6
DER	1271	4	142.2	102.2
TDER	1275	0	68.2	91.5

Table 1. Comparison for STA/LTA, DER and TDER picks for the microseismic dataset.

before peak amplitude. As L_{sw} increases from 0.4 to 0.7s, the onset energy decreases slowly, which indicates that as the window increases, the calculated energy includes not only the onset energy, but also the noise energy. The inflection point in Fig. 9b is corresponding to the window length that can cover onset energy. Thus, this optimal L_{sw} was set to 0.3 s in experiments using microseismic data.

The selection of the window length (L_{sw}) on arrival time picking was further evaluated through the microseismic data. We have tested the variations of STD and MAD between TDER and manual picks for different values of L_{lw} for a range of L_{sw}. In the end, the results of MAD and STD with varying L_{sw} from 0.1 s to 0.7s and L_{lw} equal to 1.2 s, were used to illustrate the parameter selection (Fig. 9c-d). Due to the small window length caused by setting L_{sw} of 0.1 s, there is a higher occurrence of outliers and both MAD and STD give high values. When L_{sw} increases to 0.2 s, both STD and MAD go down. Then with increasing the window length from 0.2 s to 0.7 s, STD and MAD show different trends. The STD falls and tends to be a relatively stable level as the

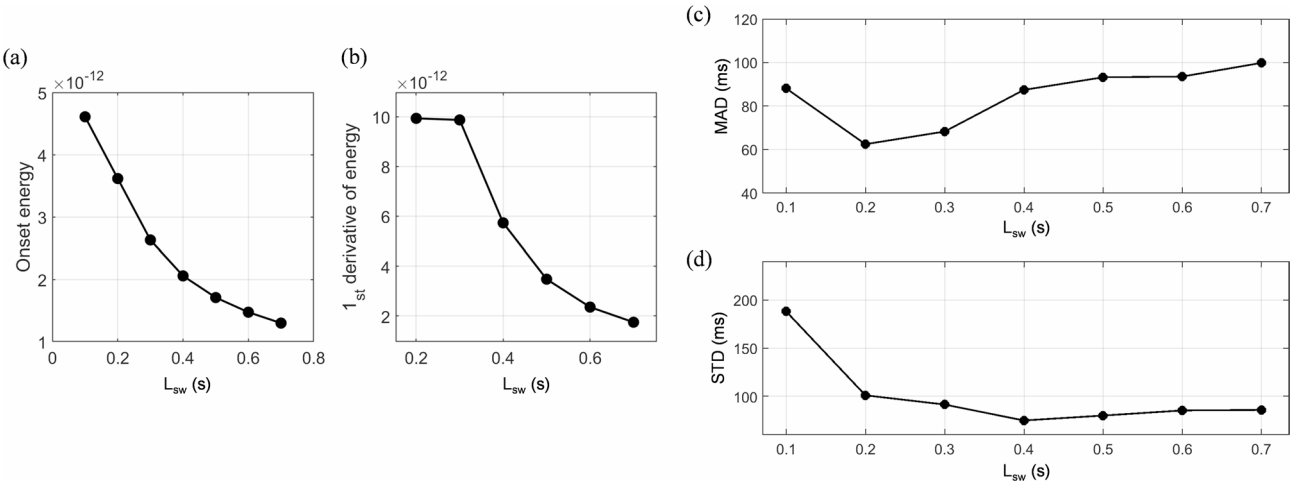

Fig. 9. Test results of L_{sw} on microseismic data. (**a**) Average onset energy and (**b**) first derivative of the average onset energy of microseismic data as a function of variations in L_{sw}. (**c**) MAD and (**d**) STD values as a function of variations in L_{sw}.

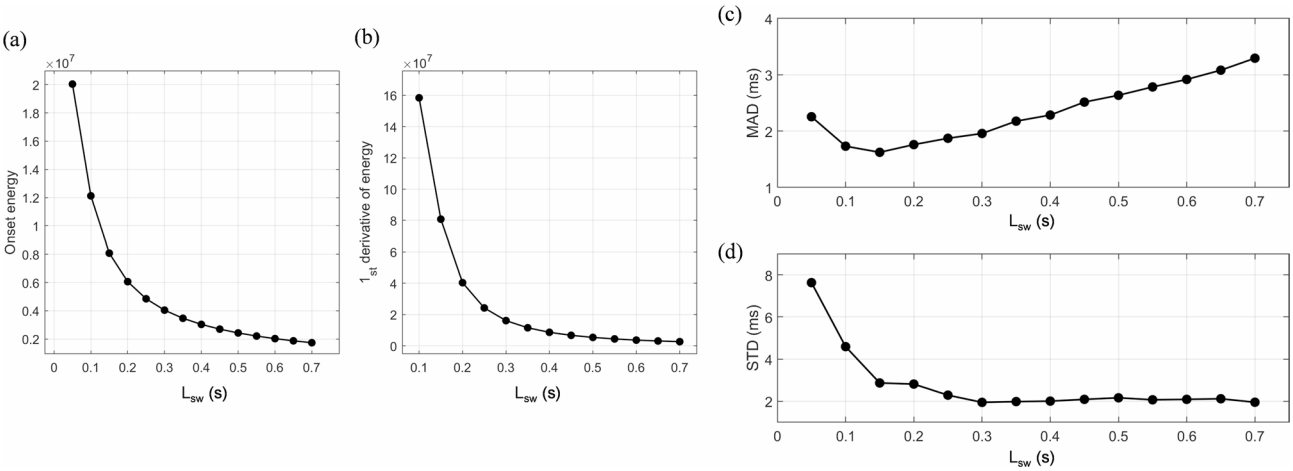

Fig. 10. Test results of L_{sw} on active tomography data. (**a**) Average onset energy and (**b**) first derivative of the energy of active tomography data as a function of variations in L_{sw}. (**c**) MAD and (**d**) STD values as a function of variations in L_{sw}.

number of outliers declines with increasing L_{sw}. However, the MAD rises as the seismogram energy variations become less sensitive to the TDER as L_{sw} increases. Therefore, setting L_{sw} to be 0.3 s, both MAD and STD give relatively low values.

The proposed method to determine L_{sw} was also validated on active tomography data (Fig. 10). Variations of the average onset energy of tomography data with different L_{sw} are shown in Fig. 10a. In each trace, the onset energy is calculated using the section of signal with the length of L_{sw} before peak amplitude. When L_{sw} is 0.05 s to 0.2 s with the step of 0.05 s, onset energy decreases rapidly, which shows that the onset energy mainly locates in these window lengths before peak amplitude. As L_{sw} increases from 0.2 to 0.7s, the onset energy decreases slowly, which indicates that as the window increases, the calculated energy includes not only the onset energy, but also the noise energy. The inflection point in Fig. 10b is corresponding to the window length that can cover onset energy. Thus, L_{sw} is proper to be set at around 0.2 s in TDER method for this tomography data. The selection of L_{sw} was proved by the MAD and STD of picking results (Fig. 10c-d). When L_{sw} is around 0.2 s, both MAD and STD give relatively low values.

The two datasets have different optimal L_{sw} and it suggests that L_{sw} is a data-based parameter. By comparing the dominant frequency of two datasets provided in the previous section 'Overview of field data', the data show that the data with higher dominant frequency results in shorter L_{sw}. For microseismic data, the optimal L_{sw} is about 12 times of dominant period; for tomography data, the optimal L_{sw} is about 14 times of dominant period. The number of times of dominant period for two datasets has similar value. Thus, the parameter L_{sw} should be related to the frequency content of the signals.

The noise energy is assessed using the second and third windows with the same length of L_{lw}. It is suggested that, for microseismic data picking, L_{lw} needs to be several times greater than L_{sw}[48–50]. With the increase of L_{lw}, E_2 and E_3 tend to be more similar, resulting in the DER' approaching zero in noisy areas. The MAD and STD are illustrated in Fig. 11a-b with L_{lw} progressively rises from 0.3 s, which is equivalent to L_{sw}, to 1.5 s. If L_{lw} stays at excessively small values, noise cannot be adequately suppressed, resulting in noticeable DER' variations within noise-dominant regions and TDER misidentification of seismic onset. When L_{lw} is less than 1.2 s, many outliers appear, resulting in high MAD and STD values. However, as L_{lw} increases from 1.2 s to 1.5 s, both MAD and STD rise rapidly. Therefore, the graphs indicate that L_{lw} with four times of L_{sw} produces the best results and we use L_{lw} =1.2s in experiments using microseismic data.

Next, we evaluated the sensitivity of the transformation window length used in the TDER computation. As introduced in the previous section 'Detection of arrival time', the transformation removes a linear trend from the DER' over a window of length $2L_{sw}$ located before the maximum point of DER'. This is done to make the DER' values at both ends of the window zero, transforming the onset point into a global minimum. To assess the robustness of this choice, we varied the scaling coefficient N such that the window length becomes $N \times 2$Lsw, and examined how this affects the picking accuracy in terms of MAD and STD. The test range for N was set between 0.6 and 1.4 with a step size of 0.2 to evaluate its impact on the results (Fig. 11c-d). This test was conducted using a fixed L_{sw} = 0.3 s and L_{lw}= 1.2 s. Different from the window length settings, $2L_{sw}$ carries intrinsic meaning, and the results showed that the sensitivity to variations in N is relatively low.

Future research on improvement of TDER method

False alarms are often due to irregular noise, such as spikes, before the target event's onset, since the multiwindow method of DER is based on the assumption of random noise[43]. Therefore, TDER method also faces this limitation, because both methods use the same characteristic function to extract the feature of data. To mitigate this limitation, a proper method should be proposed to remove spikes. Here we have performed an initial test by using the Hampel filter[51] to remove spikes before picking. The Hampel filter is a robust statistical technique used to identify and remove outliers in data. It operates by comparing each data point to the median of a surrounding window, with a threshold set by the Median Absolute Deviation (MADV), a robust measure of variability. Data points that deviate from the local median by more than a predefined number of MADVs are classified as outliers. Spike noise manifests as sudden, short-duration deviations from the surrounding signal. The Hampel filter is effective at removing such spikes because it directly targets these statistically anomalous points without distorting the underlying trend. Figure 12 shows an example of picking improvement using Hampel filter for the case when spikes appear in the recording. Using this filtering, the onset of the signal does not show noticeable difference compared to the original trace (Fig. 12a-b). After removing the spikes, the picking error of TDER decreases, from 278.9 ms down to 44.1 ms. However, the STA/LTA and DER picks remain at a similar level to the ones before filtering, and do not show any improvement on picking (Fig. 12c-j). The comparison further proves the adaptivity and advantage of TDER picking strategy. Therefore, the initial test with Hampel filtering suggests potential for improvement when combined with appropriate preprocessing strategies. In future research, the Hampel filter can be consistently applied across the experiments and a broader quantitative evaluation would be necessary to justify its effectiveness.

Conclusion

This study proposes a detection strategy for determining arrival times of noisy microseismic data. An energy-based method was used to implement the detection strategy. The algorithm minimizes the effect of noise and accurately detects the arrival time using a transformation function. The DER', derived from DER, extracts the

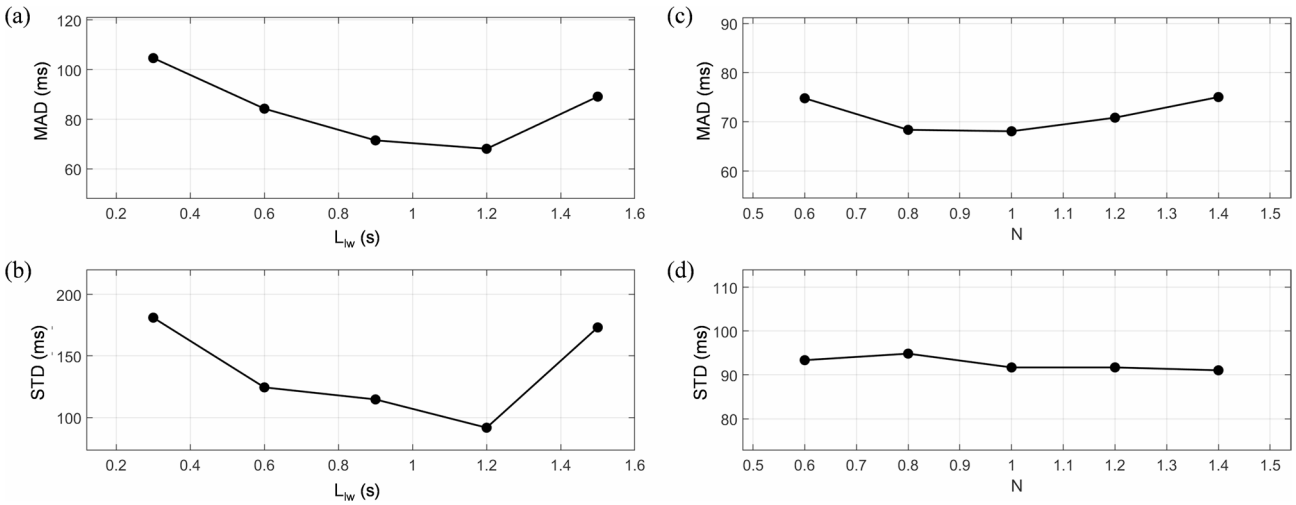

Fig. 11. Test results of different parameters on microseismic data. (**a**) MAD and (**b**) STD values as a function of variations in L_{lw}. (**c**) MAD and (**d**) STD values as a function of variations in N.

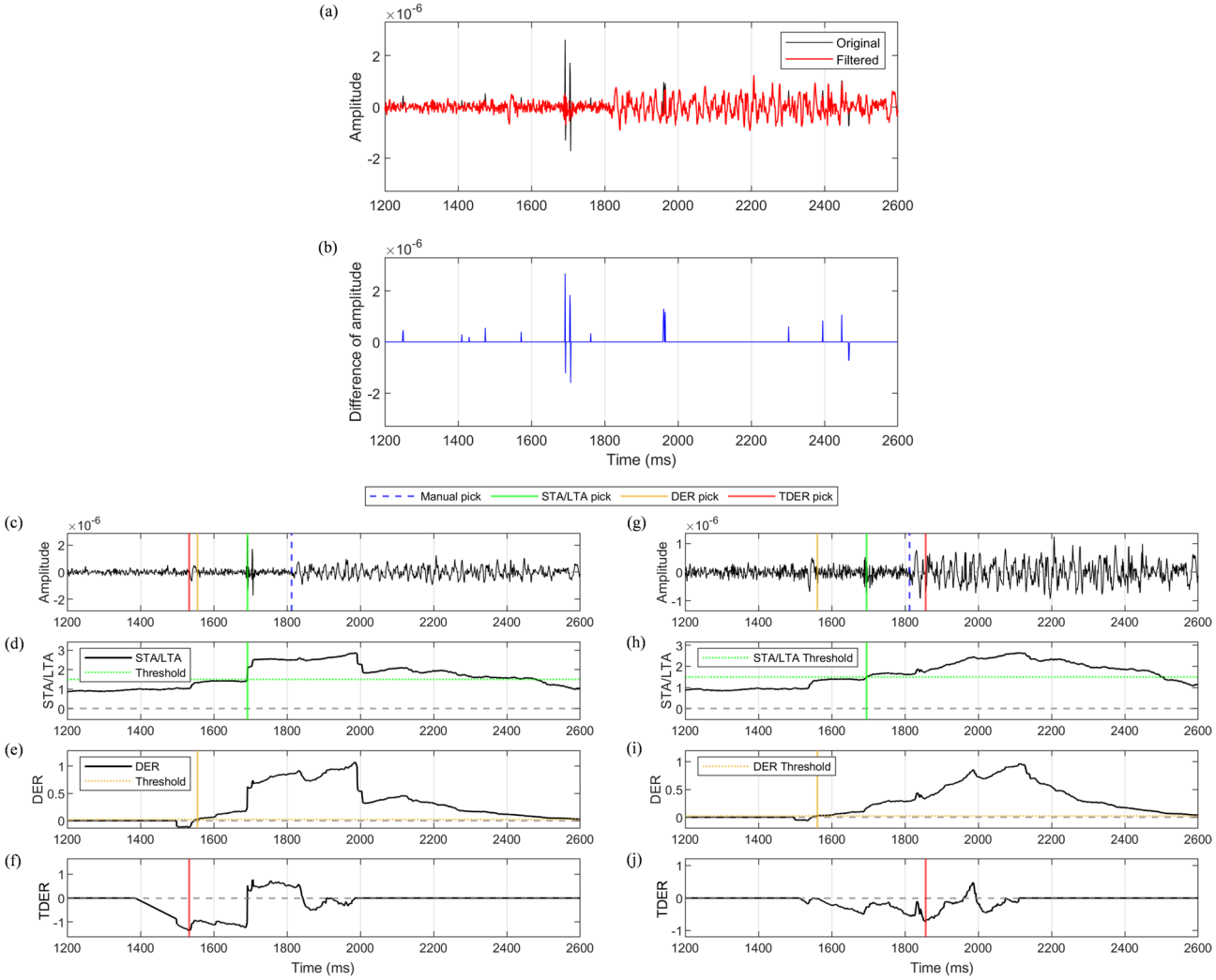

Fig. 12. An example of picking improvement using Hampel filter. (**a**) Comparison of an original seismic trace (black) and filtered seismic trace (red). (**b**) Difference of amplitude between original seismic trace and filtered seismic trace in (**a**). (**c**) Original seismic trace with manual, STA/LTA, DER and TDER picks and (**d**)-(**f**) its STA/LTA, DER and TDER values, respectively. (**g**) Filtered seismic trace with manual, STA/LTA, DER and TDER picks and (**h**)-(**j**) its STA/LTA, DER and TDER values, respectively.

change from noise to signal and TDER mimic the human operator to transform the point of the noise-signal change to the minimum and easily detect it.

The TDER algorithm's accuracy was demonstrated qualitatively and quantitatively by implementing it to both pseudo-synthetic and field data. The pseudo-synthetic data were generated by adding adjusted real noise to the field data with high SNR. The results confirmed that the TDER algorithm performs better than STA/LTA and DER methods for noisy scenarios. The noise effect on picking was also analyzed by using the ratio of delayed picks between TDER picks and the manual picks and the results suggested that the ratio of delayed picks did not decrease linearly with increasing the noise level. Based on the noise tests, the STD of picking error could be used as an estimate of the picking uncertainty. Future research should be done to validate this estimation. Estimation of picking accuracy is useful for future location of seismic event, which would benefit the evaluation and analysis of location results. For the tests on field data obtained in microseismic monitoring on an unstable rock face, we compared TDER's performance with that of the STA/LTA and DER methods. The comparison results show the improvement of picking accuracy and the reduction of failure detections by using the TDER algorithm, due to the adaptive feature of the detection strategy.

Sensitivity analysis and parameter selection have also been performed. The short window's length needs to represent the onset energy of target signal, as revealed by the calculation of onset energy; the lengths of the two long windows should represent the energy of background noise and be set to fourfold that of the short window; the transformation window's length should be twofold that of the short window and be located just before the peak point of TDER. The initial test using Hampel filter to remove spikes suggests potential for improvement on picking accuracy of TDER, and future work on a broader quantitative evaluation would be necessary. Further improvement in future work can be done by combining our method with other techniques to distinguish between

P- and S-waves and comparing our method with other picking methods, such as AIC method. Therefore, the developed algorithm features a relatively simple parameterization and is expected to be easily adaptable across various microseismic monitoring networks. Moreover, the proposed arrival time detection strategy could be applied to other picking methods instead of thresholding strategy.

Data availability

The datasets generated during and/or analysed during the current study are available from the corresponding author on reasonable request.

Received: 24 February 2025; Accepted: 29 September 2025
Published online: 04 November 2025

References

1. Billings, S. D., Sambridge, M. S. & Kennett, B. L. N. Errors in hypocenter location: picking, model, and magnitude dependence. *Bull. Seismol. Soc. Am.* **84**, 1978–1990 (1994).
2. Colombero, C., Comina, C., Vinciguerra, S. & Benson, P. M. Microseismicity of an unstable rock mass: from field monitoring to laboratory testing. *J. Geophys. Res. : Solid Earth.* **123**, 1673–1693 (2018).
3. Hafez, A. G., Khan, T. A. & Kohda, T. Earthquake onset detection using spectro-ratio on multi-threshold time–frequency sub-band. *Digit. Signal. Process.* **19**, 118–126 (2009).
4. Stewart, S. W. Real-time detection and location of local seismic events in central California. *Bull. Seismol. Soc. Am.* **67**, 433–452 (1977).
5. Zhang, Z., Arosio, D., Hojat, A. & Zanzi, L. Tomographic experiments for defining the 3D velocity model of an unstable rock slope to support microseismic event interpretation. *Geosci. (Switzerland).* **10**, 1–23 (2020).
6. Zhang, Z., Arosio, D., Hojat, A. & Zanzi, L. Reclassification of microseismic events through hypocenter location: case study on an unstable rock face in Northern Italy. *Geosci. (Switzerland).* **11**, 1–20 (2021).
7. Zhang, Z., Arosio, D., Hojat, A. & Zanzi, L. Designing the expanded microseismic monitoring network for an unstable rock face in Northern Italy. *Pure Appl. Geophys.* **179**, 1623–1644 (2022).
8. Benavente, D., Galiana-Merino, J. J., Pla, C., Martinez-Martinez, J. & Crespo-Jimenez, D. Automatic detection and characterisation of the first P- and S-wave pulse in rocks using ultrasonic transmission method. *Eng. Geol.* **266**, 105474 (2020).
9. Verdon, J. P., Kendall, J. M., White, D. J. & Angus, D. A. Linking microseismic event observations with Geomechanical models to minimise the risks of storing CO2 in geological formations. *Earth Planet. Sci. Lett.* **305**, 143–152 (2011).
10. Will, R., Smith, V., Leetaru, H. E., Freiburg, J. T. & Lee, D. W. Microseismic monitoring, event occurrence, and the relationship to subsurface geology. in *Energy Procedia*. 63, 4424–4436 (Elsevier Ltd, 2014).
11. Li, P. X., Feng, X. T., Feng, G. L., Xiao, Y. X. & Chen, B. R. Rockburst and microseismic characteristics around lithological interfaces under different excavation directions in deep tunnels. *Eng. Geol.* **260**, 105209 (2019).
12. Lu, A. et al. Numerical simulation study on microseismic characteristics and rockburst hazard prediction in deep mining of steeply inclined coal seams. *Rock Mech. Rock. Eng* (2024).
13. Poliannikov, O. V., Malcolm, E., Djikpesse, A., Prange, M. & H. & Interferometric hydrofracture microseism localization using neighboring fracture. *Geophysics* **76**, WC27–WC36 (2011).
14. Zhao, C., Zhang, Z. & Lei, Q. Role of hydro-mechanical coupling in excavation-induced damage propagation, fracture deformation and microseismicity evolution in naturally fractured rocks. *Eng. Geol.* **289**, 106169 (2021).
15. Ma, K., Tang, C. A., Xu, N. W., Liu, F. & Xu, J. W. Failure precursor of surrounding rock mass around cross tunnel in high-steep rock slope. *J. Cent. South. Univ.* **20**, 207–217 (2013).
16. Salvoni, M. & Dight, P. M. Rock damage assessment in a large unstable slope from microseismic monitoring - MMG century mine (Queensland, Australia) case study. *Eng. Geol.* **210**, 45–56 (2016).
17. Ma, K., Tang, C. A., Liang, Z. Z., Zhuang, D. Y. & Zhang, Q. B. Stability analysis and reinforcement evaluation of high-steep rock slope by microseismic monitoring. *Eng. Geol.* **218**, 22–38 (2017).
18. Xu, N. W. et al. Microseismic monitoring and stability evaluation for the large scale underground caverns at the Houziyan hydropower station in Southwest China. *Eng. Geol.* **188**, 48–67 (2015).
19. Arosio, D., Longoni, L., Papini, M. & Zanzi, L. Analysis of microseismic activity within unstable rock slopes. in Modern Technologies for Landslide Monitoring and Prediction (ed Scaioni, M.) 141–154 (Springer Berlin Heidelberg, (2015).
20. Yfantis, G., Pytharouli, S., Lunn, R. J. & Carvajal, H. E. M. Microseismic monitoring illuminates phases of slope failure in soft soils. *Eng. Geol.* **280**, 105940 (2021).
21. Sabbione, J. I. & Velis, D. R. A robust method for microseismic event detection based on automatic phase pickers. *J. Appl. Geophys.* **99**, 42–50 (2013).
22. Sleeman, R. & van Eck, T. Robust automatic P-phase picking: an online implementation in the analysis of broadband seismogram recordings. *Phys. Earth Planet. Interiors*. **113**, 265–275 (1999).
23. Leonard, M. Comparison of manual and automatic onset time-picking. *Bull. Seismol. Soc. Am.* **90**, 1384–1390 (2000).
24. Akram, J. & Eaton, D. W. Refinement of arrival-time picks using a cross-correlation based workflow. *J. Appl. Geophys.* **135**, 55–66 (2016).
25. Senkaya, M. & Karslı, H. A semi-automatic approach to identify first arrival time: the cross-correlation technique (CCT). *Earth Sci. Res. J.* **18**, 107–113 (2014).
26. Anikiev, D. et al. Machine learning in microseismic monitoring. *Earth Sci. Rev.* **239**, 104371 (2023).
27. Zhu, W., Beroza, G. C. & PhaseNet A deep-neural-network-based seismic arrival time picking method. *Geophys. J. Int.* **216**, 261–273 (2019).
28. Li, J., Stankovic, L., Pytharouli, S. & Stankovic, V. Automated platform for microseismic signal analysis: Denoising, detection, and classification in slope stability studies. *IEEE Trans. Geosci. Remote Sens.* **59**, 7996–8006 (2021).
29. Wang, J., Xiao, Z., Liu, C., Zhao, D. & Yao, Z. Deep learning for picking seismic arrival times. *J. Geophys. Res. : Solid Earth.* **124**, 6612–6624 (2019).
30. Chen, G., Li, J. & CubeNet Array-based seismic phase picking with deep learning. *Seismol. Res. Lett.* **93**, 2554–2569 (2022).
31. Feng, T., Mohanna, S., Meng, L. & EdgePhase A deep learning model for multistation seismic phase picking. *Geochem Geophys. Geosyst* **23**, (2022).
32. Anant, K. S. Dowla. Wavelet transform methods for phase identification in three-component seismograms. *Bull. Seismol. Soc. Am.* **87**, 1598–1612 (1997).
33. Leonard, M. Kennett B.L.N. Multi-component autoregressive techniques for the analysis of seismograms. *Phys. Earth Planet. Inter.* **11**, 247–263 (1999).
34. Saragiotis, C. D., Hadjileontiadis, L. J. & Panas, S. M. PAI-S/K: A robust automatic seismic P phase arrival identification scheme. *IEEE Trans. Geosci. Remote Sens.*, (2002).

35. Hafez, A. G., Rabie, M. & Kohda, T. Seismic noise study for accurate P-wave arrival detection via MODWT. *Comput. Geosci.* **54**, 148–159 (2013).
36. Gaci, S. The use of wavelet-based denoising techniques to enhance the first-arrival picking on seismic traces. *IEEE Trans. Geosci. Remote Sens.* **52**, 4558–4563 (2014).
37. Mikesell, T. D., Van Wijk, K., Ruigrok, E., Lamb, A. & Blum, T. E. A modified delay-time method for statics Estimation with the virtual refraction. *Geophysics* **77**, A29–A33 (2012).
38. Allen, R. V. Automatic earthquake recognition and timing from single traces. *Bull. Seismol. Soc. Am.* **68**, 1521–1532 (1978).
39. Coppens, F. First arrival picking on Common-Offset trace collections for automatic Estimation of static corrections. *Geophys. Prospect.* **33**, 1212–1231 (1985).
40. Han, L. Microseismic monitoring and hypocenter location (University of calgary, 2010).
41. Lee, M., Byun, J., Kim, D., Choi, J. & Kim, M. Improved modified energy ratio method using a multi-window approach for accurate arrival picking. *J. Appl. Geophys.* **139**, 117–130 (2017).
42. Khalaf, A., Camerlynck, C., Florsch, N. & Schneider, A. Development of an adaptive multi-method algorithm for automatic picking of first arrival times: application to near surface seismic data. *Near Surf. Geophys.* **16**, 507–526 (2018).
43. Kim, D., Joo, Y. & Byun, J. First-Break picking method based on the difference between multiwindow energy ratios. *IEEE Trans. Geosci. Remote Sens.* **61**, 5905510 (2023).
44. Akram, J. & Eaton, D. Adaptive microseismic event detection and automatic time picking. *GeoConvention* 1–5 (2012).
45. Lomax, A., Michelini, A., Curtis, A. & Earthquake Location Direct, Global-Search methods. in Encyclopedia of Complexity and Systems Science (ed. 1–33 (Springer, New York, (2014).
46. Spillmann, T. et al. Microseismic investigation of an unstable mountain slope in the Swiss alps. *J. Geophys. Res. : Solid Earth*. **112**, 1–25 (2007).
47. Arosio, D., Longoni, L., Papini, M., Boccolari, M. & Zanzi, L. Analysis of microseismic signals collected on an unstable rock face in the Italian prealps. *Geophys. J. Int.* **213**, 475–488 (2018).
48. Chen, Z. A multi-window algorithm for automatic picking of microseismic events on 3-C data. in *SEG Tech. Program* 1288–1291 (2005). (Society of Exploration Geophysicists.
49. Wong, J., Han, L., Bancroft, J. C. & Stewart, R. R. Automatic time-picking of first arrivals on noisy microseismic data. *CREWES Res. Report* 1–6 (2009).
50. Akram, J. & Eaton, D. W. A review and appraisal of arrival-time picking methods for downhole microseismic data. *Geophysics* **81**, KS71–KS91 (2016).
51. Pearson, R. K., Neuvo, Y., Astola, J. & Gabbouj, M. The class of generalized hampel filters, *2015 23rd European Signal Processing Conference (EUSIPCO)*, Nice, France, 2501–2505 (2015).

Acknowledgements

This work was supported by the Department of Education, Liaoning Province (Grant No. JYTMS20230801); the National Natural Science Foundation of China (Grant No. 42274129).

Author contributions

Z. Z.: Conceptualization, Methodology, Data curation, Software, Formal analysis, Investigation, Funding acquisition, Writing – original. W. C.: Visualization, Data curation, Software. S. W.: Software, Visualization, Data curation, Methodology. H. Y.: Data curation, Resources, Visualization. J. W.: Resources, Data curation, Software. D. A.: Writing – review and editing, Data curation, Investigation, Software, Supervision. A. H.: Writing – review and editing, Investigation, Supervision. L. Z.: Writing – review and editing, Data curation, Investigation, Supervision.

Declarations

Competing interests

The authors declare no competing interests.

Additional information

Correspondence and requests for materials should be addressed to Z.Z.